Politecnico di Milano

Spacecraft Attitude Dynamics
Academic Year 2023/2024

Project group n. 42

Project n. 547

Final Project Report
Attitude Control of a MiniSat

Team members:

Person code	Surname	Name	Bachelor (type and University)
10710744	Bellini	Davide	Aerospace Engineering – Politecnico di Milano
10706185	Mensi Weingrill	Edoardo	Ingegneria Aerospaziale – Università degli Studi di Padova
10765536	Mirri	Pietro	Aerospace Engineering – Politecnico di Milano
10730683	Nuccio	Gabriele	Aerospace Engineering – Politecnico di Milano

Project specifications:

	Assigned specification	**Modifications (if any)**	**Motivation for modification**
Platform	MiniSat(100 – 500 kg)	~	~
Attitude parameters	Direction cosines	~	~
Mandatory sensor	Gyroscope	Extra sensors: Magnetometer and sun sensor	To determine in a simpler way the attitude of the S/C and to achieve better control
Actuators	3 magnetic coils	Extra actuator: A reaction wheel	To perform the control around the three principal inertia axis and for slew manoeuvre control

Table of contents

1. Introduction

1.1. Orbit determination

The aim of this report is to analyze the attitude dynamics and control of a MiniSat.

At first, an orbit was designed, drawing inspiration from the literature on MiniSat and aligning with the mandatory specifications of the mission. The designed orbit is a polar circular Sun-synchronous low Earth orbit, as illustrated below.

a	7100.985 km
e	0
i	98.3°
Ω	270°
ω	0°
θ	0°

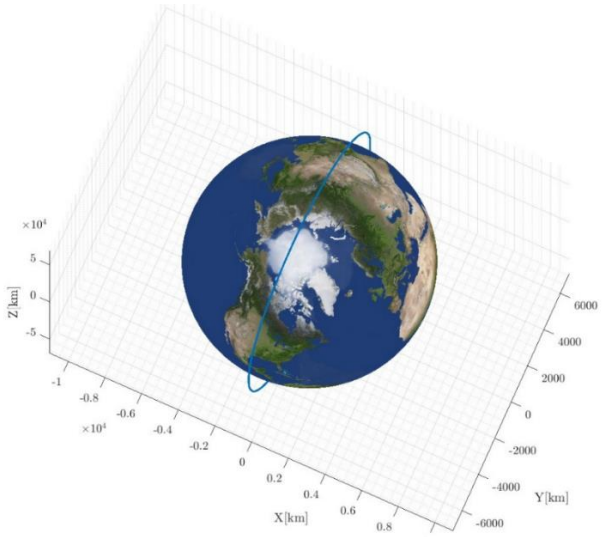

Figure 1: Orbit

The orbit was determined using the Sun-syncronous law to define the semimajor axis of the orbit.

$$\dot{\alpha}_{SUN} = \dot{\Omega}_{J2}$$

Where $\dot{\Omega}_{J2} = -\frac{3}{2}\frac{\sqrt{\mu_E}\, J_2\, R_E^2}{(1-e^2)^2\, a^{\frac{7}{2}}}\cos(i)$ and $\dot{\alpha}_{SUN} = \frac{2\pi}{365.25 \cdot 24 \cdot 3600}$

1.2. Structure properties

The MiniSat structure is characterised by the following parameters. Its primary structure measures 1.2x1x0.8 *m* and weighs 148.5 kg, featuring a solar panel situated on the lower surface measuring 1.2x1x0.04 *m* and weighing 1.5 kg. These specifications are utilized to calculate the inertia matrix:

$$\mathrm{J} = \begin{bmatrix} 20.4202 & 0 & 0 \\ 0 & 25.9202 & 0 \\ 0 & 0 & 30.5 \end{bmatrix} \mathrm{kg}\, m^2$$

Finally, the centre of gravity is defined at x_{CG} = [0 0 0] because the distribution of mass in the volume is assumed to be uniform to simplify the evaluation of the disturbances.

1.3. Mission analysis

The overall mission necessitates the execution of several critical spacecraft maneuvers, including Target Tracking, De-Tumbling, Slew Maneuver, and 3-axis stabilization. Throughout the mission, the spacecraft is tasked with Earth Nadir pointing, a requirement maintained continuously. This objective is achieved through a sequence of three control modes:

1. **De-Tumbling:**
   Purpose: Stabilizing the spacecraft by reducing angular velocity to zero.

2. **Slew manoeuvre:**
   Purpose: Performing attitude adjustments with respect to a target reference in the inertial frame after changing the pointing direction.

3. **3-axis stabilization**:
   Purpose: Maintaining stable orientation during the remainder of the mission

Additionally, the spacecraft demonstrates the capability to estimate its current attitude by synthesizing information from onboard sensors. Furthermore, it exercises control over its attitude by issuing commands to its actuators, ensuring precise and responsive adjustments throughout the mission duration.

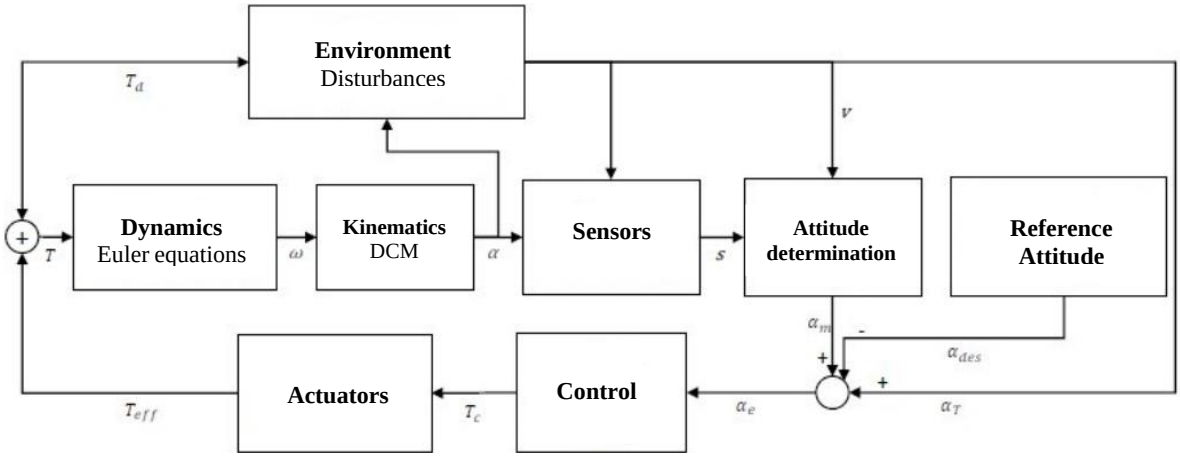

Figure 2: Architecture

Based on the manoeuvres and on the orbit designed, sensors and actuators can be chosen, in according to their capabilities.
The satellite is equipped with:

• **Attitude sensors**: Sun sensor, Magnetometer, Gyroscope
• **Actuators**: a set of 3 Magnetic Torquers and 1 Reaction Wheel

2. Model description

2.1. Spacecraft dynamics

The subsequent analysis illustrates the methodology for ascertaining spacecraft dynamics. Commencing with the definition of the initial angular velocity vector, it was adopted a conventional assumption for MiniSat in Low Earth Orbit (LEO) after the conclusion of the De-Tumbling manoeuvre.

$$\underline{\omega}_0 = \begin{bmatrix} 0.08 \\ 0.08 \\ 0.08 \end{bmatrix} rad/s$$

The attitude of the S/C is computed by integrating Euler's Equations:

$$J\underline{\dot{\omega}} = J\underline{\omega} \wedge \underline{\omega} + \underline{M_c} + \underline{M_d}$$

where ω: angular velocity, M_d: disturbance torque and M_c: control torque.
In the principal inertia axes the equations become a system of three decoupled equations:

$$\begin{cases} \underline{\dot{\omega}}_x = \dfrac{(J_y - J_z)}{J_x}\omega_z\omega_y + \dfrac{M_{cx}}{J_x} + \dfrac{M_{dx}}{J_x} \\ \underline{\dot{\omega}}_y = \dfrac{(J_z - J_x)}{J_x}\omega_x\omega_z + \dfrac{M_{cy}}{J_y} + \dfrac{M_{dy}}{J_y} \\ \underline{\dot{\omega}}_z = \dfrac{(J_x - J_y)}{J_z}\omega_x\omega_y + \dfrac{M_{cz}}{J_z} + \dfrac{M_{dz}}{J_z} \end{cases}$$

Once the equations are integrated it can be extracted the $\underline{\omega}$ which is the angular velocity in the body reference frame to then use it to evaluate the orientation of the spacecraft.

2.2. Orientation with DCM

To delineate the orientation of the body reference frame in space with respect to the inertial frame, a Direction Cosine Matrix (DCM) has been assigned. Starting from the previous definition of angular velocity vector, first we compute the $\omega \wedge$ matrix as:

$$\omega \wedge = \begin{bmatrix} 0 & -\omega_3 & \omega_2 \\ \omega_3 & 0 & -\omega_1 \\ -\omega_2 & \omega_1 & 0 \end{bmatrix}$$

Then, it was imposed a guess on the initial attitude matrix of the spacecraft to obtain the desired orientation of the body frame with respect to the LVLH frame, the matrix must be orthogonal due to the constraint of the DCM.

$$A_0 = \begin{bmatrix} -\cos(\varphi) & -\sin(\varphi) & 0 \\ 0 & 0 & 1 \\ -\sin(\varphi) & \cos(\varphi) & 0 \end{bmatrix}$$

It's possible to get the $\dot{A}$ multiplying the previous equations:

$$\dot{A} = -\omega \wedge \mathrm{A}$$

Now A is determined at every time instant by just integrating this equation.
To understand how attitude parameters evolve over time, it is necessary to employ orthogonalization, using a first-order approximation.

$$A(t) = \frac{3}{2}A_0(t) - \frac{1}{2}A_0(t)A_0^T(t)A_0(t)$$

From now on the attitude matrix is indicated as $A_{B/N}$

2.3. Further consideration on reference frame

Since the evaluation of the mission has a different time scale with respect to the orbital mechanics analysis, a simplified is applied only to propagate the true anomaly, this is justified since the simulation time is small, in the order of two orbits, so the other term effects on the other Keplerian elements are considered negligible.
Since the orbit is circular the true anomaly variation can be evaluated as:

$$\theta = nt \quad \text{where } n = \sqrt{\frac{\mu_E}{a^3}}$$

with a: semimajor axis of the S/C orbit and μ_E: the Gravitational constant of the Earth.
Considering the circular orbit, it can be founded the position vector in the inertial reference frame as:

$$r_N = a\begin{bmatrix}\cos(\theta)\\ \sin(\theta)\\ 0\end{bmatrix}$$

3. Disturbance Torques

To try to realize a real system, disturbance torques due to the environment where the S/C moves are modelled. By aligning with the predetermined orbit parameters, certain discernments can be made, facilitating the simplification of the intricate model to yield optimal outcomes. Consequently, within the spectrum of diverse disturbances, it is possible to remove one of these: at high altitude, aerodynamic drag doesn't give an important contribution. Due to the altitude is almost 730 km, the effect of this perturbation is negligible with respect to the others, given its value is orders of magnitude smaller than those of the alternative perturbations.
At 730 km $\rho = 2.16 \times 10^{-17}$ and considering a mean value of drag coefficient that is $c_D \approx 2.2$. The torque can be estimated as:

$$T_{aero} = -\underline{r} \wedge \frac{1}{2}\rho c_D v_{rel}^2 \frac{\underline{v}_{rel}}{\|\underline{v}_{rel}\|} A_{cross} \approx 10^{-14}/10^{-15}$$

Where v_{rel} is the relative velocity of the spacecraft with respect to the atmosphere and A_{cross} is the cross section perpendicular to the relative velocity.
During the simulation, to simplify again the model, an analysis about the behavior of the other disturbances has been made.
The model includes three types of disturbance torques which includes the three most important torques usually analyzed:

- **Solar radiation pressure torque:**
  Due to the different sources of electromagnetic radiation in the orbit of interest.
- **Magnetic torque:**
  Due to the magnetic field of the Earth.
- **Gravity gradient torque:**
  Due to the position, and orientation and characteristics of the S/C.

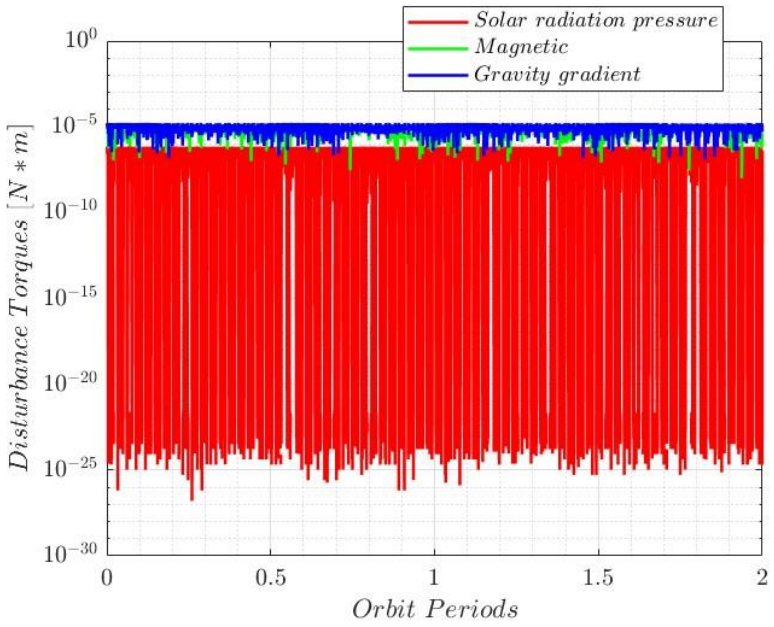

Figure 3: Disturbance torques.

As the Figure 3 shows, Gravity Gradient and Magnetic Field are the most important disturbance sources, it has been preferred so to consider only these ones in order to simplify the model.

3.1. Solar radiation pressure

The outer surface of a satellite is illuminated by solar radiation, resulting in the generation of pressure. This pressure, in turn, produces both a force and a torque around the center of mass of the satellite. These effects arise from three primary contributions:

- Direct solar radiation
- Radiation reflected by the Earth
- Earth radiation.

The first contribution is practically constant with altitude while the last two contributions are strongly dependent on the altitude and were computed using a simple linear interpolation consider the altitude $h \approx 750\ km$.
The power per unit surface become:

$$F_e = (1358 + 550 + 135)\frac{W}{m^2} = 2043\frac{W}{m^2}$$

Then, the average pressure due to the radiation can be evaluated as:

$$P = \frac{F_e}{c} = 6.8147\ \mu\text{Pa}$$

Where c is the speed of light.
The electromagnetic radiation model was computed by breaking down the external structure of the spacecraft into a series of flat surfaces. Each surface is defined by its normal unit vector $\hat{N}_i$ and is linked to specific specular and diffuse reflection coefficients.
By defining a matrix containing the normal unit vector:

$$\hat{N} = \begin{bmatrix} 1 & 0 & -1 & 0 & 0 & 0 \\ 0 & 1 & 0 & -1 & 0 & 0 \\ 0 & 0 & 0 & 0 & 1 & -1 \end{bmatrix}$$

And the reflection coefficient as:

	Spacecraft	Panel
ρ_s	0.5	0.1
ρ_d	0.1	0.1

Table 1

To compute the torque is now necessary to evaluate at first the Sun direction in the inertial frame. Once the position vector of the MiniSat with respect to the Earth is evaluated, then to be more precise, also the position vector of the Earth with respect to the Sun was estimated starting from the true anomaly:

$$\dot{\theta_s} = \frac{n_s(1 + e_s \cos(\theta_s))^2}{(1 - e_s^2)^{3/2}}$$

where n_s is the mean angular velocity of the Earth around the Sun and e_s: eccentricity of the Earth orbit. Consequently, by integrating the equation above:

$$\underline{\hat{S}}_N = r_S \begin{bmatrix} \cos(\theta_s) \\ \sin(\theta_s)\cos(\varepsilon) \\ \sin(\theta_s)\sin(\varepsilon) \end{bmatrix} \rightarrow \ \underline{\hat{S}}_B = A_{B/N}\, \underline{\hat{S}}_N$$

Where r_S is the position vector of the Earth with respect to the Sun and ε is the ecliptic inclination and is equal to 23.45°.
Then the Torque is evaluated as:

$$\underline{M_d}_{SRP} = -\sum_{i=1}^{n} \underline{r}_{Fi} \wedge PA_i(\hat{S}_B \cdot \hat{N}_i) \left[(1 - \rho_s)\hat{S}_B + \left(2\rho_s(\hat{S}_B \cdot \hat{N}_i) + \frac{2}{3}\rho_d\right)\hat{N}_i\right]$$

Where $\underline{r}_{Fi}$ are the moment arms determined considering the centre of the forces as the centre of the S/C and A_i are the flat surfaces areas.

3.2. Gravity gradient

The gravitational field exhibits non-uniformity across the spacecraft's volume, potentially giving rise to a torque on the satellite. Its effect along the three principal axes can be obtained by integrating the gravitational force over the body.
In order to define the Gravity gradient, at first it should be defined a matrix that relates the LVLH frame of the Earth with respect to the inertial frame:

$$A_{L/N} = \begin{bmatrix} \cos(\theta) & \sin(\theta) & 0 \\ -\sin(\theta) & \cos(\theta) & 0 \\ 0 & 0 & 1 \end{bmatrix} \begin{bmatrix} 1 & 0 & 0 \\ 0 & \cos(i) & \sin(i) \\ 0 & -\sin(i) & \cos(i) \end{bmatrix} \begin{bmatrix} \cos(\Omega) & \sin(\Omega) & 0 \\ -\sin(\Omega) & \cos(\Omega) & 0 \\ 0 & 0 & 1 \end{bmatrix}$$

$$A_{B/L} = A_{B/N}\, A_{L/N}^T \rightarrow \begin{bmatrix} c_1 \\ c_2 \\ c_3 \end{bmatrix} = A_{B/L} \begin{bmatrix} 1 \\ 0 \\ 0 \end{bmatrix}$$

Now the torque is computed as:

$$\underline{M_d}_{GG} = \frac{3\mu_E}{r^3} \begin{Bmatrix} (I_z - I_y)c_2c_3 \\ (I_x - I_z)c_1c_3 \\ (I_y - I_x)c_1c_2 \end{Bmatrix}$$

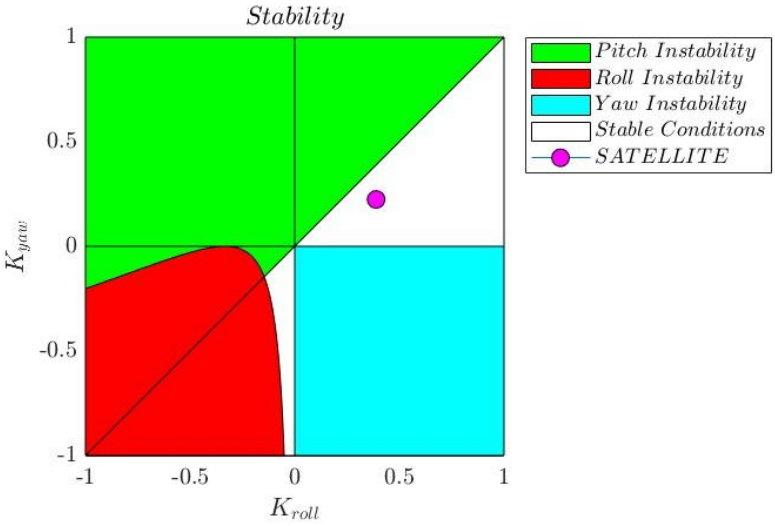

Figure 4

Further considerations are made looking at the stability conditions expressed by the stability region diagrams showed in the *Figure 4*. It's necessary to stay in the white region to maintain stability once the gravity gradient torque is included in the model.

3.3. Magnetic torque

The Earth's magnetic field can be conceptualized as one produced by a dipole inclined at an 11.5° angle to the Earth's axis. This magnetic field is dynamic, exhibiting characteristics such as a slow rotation, time-varying amplitude reduction, higher intensity at the poles, and attenuation with greater distance from the Earth's surface. In alignment with the designated orbit, the complete 13th order model of the International Geomagnetic Reference Field (IGRF) was modelled. The Gaussian coefficients g_n^m and h_n^m are subjected to time variation over the years and their experimental value is known up to 13th order. The magnetic disturbance torque is caused by the interaction between Earth's magnetic field and the residual magnetic induction due to on-board currents through wirings or electronics. The residual dipole was estimated thanks to NASA SP-8018 [6] and is related to the function of the Spacecraft (spinning or non-spinning) and to its mass:

$$\underline{m} = 1.4 \times 10^{-3}[0.2\ 0.2\ 1] \cdot m\ [A\ m^2]$$

Where m is the mass of the S/C. The magnetic torque hence becomes: $\underline{M}_{d_{MAG}} = \underline{m} \wedge \underline{B}_N$
Where $\underline{B}_N$ is the magnetic field intensity approximated to the 13th order.

4. Attitude sensors

As the dynamics and attitude of the spacecraft cannot be predetermined during the mission based on previous considerations, it becomes essential to integrate sensors to assess the spacecraft's orientation and angular velocity in real-time.
A gyroscope was model as the assigned sensor for the mission, it permits the computation of the angular velocity on board. Also the attitude matrix of the MiniSat and so its orientation could be computed but this would required better knowledge on single axis determination of the attitude. The decision made was so to use other attitude sensors: a three-axis Magnetometer and a Sun sensor to establish the orientation as usual made in many applications.

4.1. Gyroscope

For this modelling, a closed loop fiber optic gyro was used. It works with a source of light that creates a light beam that passes through an optical path made in fiber optic; by measuring when the signal returns and knowing the radius of the fiber optic wire the angular velocity is estimated. The gain in using this type of gyros is having no problem in friction and motion while on the other side this could be a thick sensor, so difficult to place somewhere. The analysis did on the Gyroscopes was done considering the multiple causes that affects the measure, depending on temperature, misalignment, non-linearity, and instability and other noises.
Here are the data used in the characterization of the gyros:

FS *[deg]*	**n° of bit**	**f** *[Hz]*	**Misalignment error** *[mrad]*	**Scale factor – non-linearity** *[ppm]*	**Scale factor - repeatability** *[ppm]*	**Scale factor – asymmetry** *[ppm]*	**ARW** *[°/h^0.5]*	**Bias instability** *[°/h]*
400	*24*	*150*	*1*	*30*	*30*	*30*	*0.002*	*0.01*

Table 2: GS-FOG70A specifications [1]

The gyro errors are used to modify the angular velocity obtained by the dynamics approximation did before as: $\underline{\omega_m} = G\underline{\omega_B} + \underline{n} + \underline{b}$
Where $\underline{b} = RRW = Bias\ instability \cdot \sqrt{T_s}$ where T_s is the sample time: obtained by the inverse of the frequency, the RRW (bias random walk) is attributed to electronic noise, G is indeed a gain matrix which contains the error due to the scale factors and the misalignment. Finally, $\underline{n}$ is the angular random walk attributed to thermos-mechanical noise of the system.

4.2. Magnetometer

Then it was chosen a 3-axis satellite fluxgate magnetometer that guarantees reliable and accurate spacecraft attitude measurements. The low noise magnetometer consists of three magnetic sensors, X, Y and Z, operating independently and simultaneously. The unit consists of a "sense" (secondary) coil surrounding an inner "drive" (primary) coil that is wound around permeable core material. The phase detector identifies key harmonics, and these signals are integrated and processed to produce a highly sensitive magnetic field measurement.
Here are the data used in the characterization of the fluxgate magnetometer:

FS *[V]*	**n° of bit**	**f** *[Hz]*	**Misalignment error** *[deg]*	**Accuracy error** *[%FS]*	**Linearity error** *[%FS]*	**Sensitivity** *[μV/nT]*	**White noise** *[pT/√Hz]*
30	*24*	*5*	*0.1*	*0.75*	*0.015*	*100*	*12*

Table 3: AAC SpaceQuest MAG-3 specifications [2]

As the same as done with the gyroscope, modelling the magnetometer consists in adding some types of noise that usually influence the measurements.

4.3. Sun sensor

A sun sensor determines a spacecraft's orientation with respect to the sun. The front surface of the chosen sensor is a synthetic sapphire window with a reflective metal coating beneath. Slits are etched in the metal and sunlight passes through them and through an optical filter onto a sensor. The charge

on the photo-sensors is read by the microcontroller which processes the image and computes the sun vector. The vector and other telemetry are returned to the spacecraft through the serial interface.
To simulate the behaviour of the sun sensor it was considered a model which characterise the sun direction in the body frame with some white noises and error in misalignment. After that a control with respect to the field of view of the sensor is done.
Defined the normal direction of the sensor in the MiniSat body frame as:

$$\underline{\hat{n}} = [0\ 0\ -1]$$

The control on the sun direction consists of establish if the sun direction is within the FOV of the sensor or if it's not. If it's not the sun direction measured by the sensor becomes a zero vector.
Here are the characteristics of the sun sensor used in the treatment:

FS *[°]*	**n° of bit**	**f** *[Hz]*	**Misalignment error** *[deg]*	**Accuracy error** *[deg]*
140	*24*	*5*	*0.1*	*0.1*

Table 4: NFSS-411 specifications [3]

4.4. Filtering of the measure

The sensor outputs are inevitably affected by the presence of noise. To restrain their oscillations a simple model of a first order low pass filter was done.
The model of the filter was done considering the iteration done at the previous time instant. This affects the new measurement with a sort of gain which could be less or higher.
The gain computed are:

K magnetometer	**K sun sensor**	**K gyro**
0.75	*0.75*	*0.75*

Table 5: Filter

5. Attitude determination

In order to accurately establish the relative attitude of the satellite within the inertial frame, a problem known as Wabha's problem is computed. This process involves considering the varying precision levels of the sun and magnetic sensors, necessitating different weightings for their contributions ($\alpha_{sun} = 1$, $\alpha_{magnetic} = \frac{1}{30}$, then normalized). The matrix $A_{B/N}$(measured) is derived as $A_{B/N} =$ UMV′ where U, M, V are respectively:

- $B = \alpha_{sun} s_{sun} v^T{}_{sun} + \alpha_{magnetic} s_{magnetic} v^T{}_{magnetic}$
- U and V denote unitary orthogonal matrices, representing the eigenvectors of matrices BB^T and B^TB respectively
- $M = diag[1,\ 1,\ \det(U) \cdot \det(V)]$

These matrixes are obtained through the MATLAB function svd.
In scenarios where the Sun sensor fails to detect the Sun, rendering its data unusable for attitude determination, since the magnetic sensor alone cannot fully define the attitude, a secondary approach is implemented. In this situation the sensor output is [0 0 0]. This is used to check in which condition the S/C is and consequently decide what type of attitude determination algorithm to use. When the output of the sun sensor is zero, the attitude is computed through discrete integration of the equation: $\frac{dA(t)}{dt} = -\underline{\omega} \wedge A(t)$, with as initial condition A_0, the last attitude calculated when the sun was still visible. This method allows attitude determination even when ensuring constant Sun-pointing is not possible, such as during detumbling or specific slew manoeuvres.

6. Control

The mission's primary aim is Earth observation through Nadir pointing. To achieve this goal, three control strategies are implemented, each tailored to specific mission phases. The deployment from a dispenser can induce a high tumble rate in the order of

$\underline{\omega_0} = \begin{bmatrix} 0.08 \\ 0.08 \\ 0.08 \end{bmatrix} rad/s$ and a random initial attitude $A_{0B/N} = A_0 = \begin{bmatrix} -\cos(\varphi) & -\sin(\varphi) & 0 \\ 0 & 0 & 1 \\ -\sin(\varphi) & \cos(\varphi) & 0 \end{bmatrix}$

The first thing to do is the detumbling, that is to slow the satellite spin rate. After having achieved sufficiently slow spin rates the S/C need to be taken into nominal condition. Therefore, through a slew manoeuvre the S/C changes both the angular velocity and the attitude to the reference values. Finally, it is implemented a control law useful in the achieved nominal condition in terms of stabilization around the three principal inertia axes, where approximation due to a linear model are mostly acceptable. Two flag variables are introduced to differentiate between the satellite's phases:

- $flag_{\text{det\_slew}}$: This flag distinguishes between detumbling and slew manoeuvre. Its output is set to 1 (indicating detumbling) if $\omega > 4n$ and 0 otherwise (indicating slew manoeuvre phase).
- $flag_{\text{slew\_nom}}$: This flag distinguishes between slew manoeuvre and 3-axis stabilization. It yields an output of 1 (representing a slew manoeuvre) if both $\omega_e > 0.1n$ (angular velocity error norm) and $\alpha_e < 10°$ (angular error norm). Conversely, it outputs 0 (indicating 3-axis stabilization) otherwise.

6.1. De-Tumbling

Detumbling aims to reduce the spacecraft's spin rate. The control strategy relies on data from three magnetometers, three gyroscopes and the action of three magnetorquers. By computing the rate of change of the magnetic field in the body reference frame

$\frac{d\underline{B}}{dt} = -\underline{\omega} \times \underline{B}$, a magnetic dipole is determined to generate a control torque $\underline{m} = -k_{det} \frac{d\underline{B}}{dt}$

From this the control torque $\underline{u} = \underline{m} \times \underline{B}$.
k_{det} is the detumbling gain decided to optimize the action of magnetorquers. It is determined with the aim of obtaining a fast detumbling while avoiding a repeated saturation. This model is valid till the rate of change of the magnetic field is mostly due to the angular velocity of the S/C in the body frame. When this become comparable with the rate of change of the magnetic field due to the change in position in the orbit the model is less effective. Therefore, this control law is used until the

spacecraft's angular velocity in norm is equal to 4n after which the change due to orbit contribution is around 20%.
Upon computing the control torque, conversion to actual voltage commands for the three magnetorquers is accomplished using the equation: $\underline{V_{act}} = \underline{u}\ \frac{R_{nom}}{n_{coil}A_{coil}}$ considering the nominal resistance of the magnetorquer R_{nom}, number of coils n_{coil} and coil area A_{coil}. Each magnetorquer is positioned parallel to one of the principal axes.

6.2. Slew manoeuvre

To achieve Nadir pointing the reference attitude is the one given by the LVLH frame $A_{LVLH/N} = A_d$, rotating as $\underline{\omega_{LVLH/N}} = \underline{\omega_d} = [0; 0; n]$. After the detumbling the spacecraft as low but semi random angular velocities and a random attitude. Transitioning from random initial conditions to Nadir pointing involves using two magnetorquers and a reaction wheel. The reaction wheel is added in order to be able to generate the requested torque. Indeed, with only the three magnetorquers the torque generated would be perpendicular to the magnetic field and it was checked that this was not enough to achieve full precise control. The third magnetorquer could be activated to desaturate the reaction wheel. The control law is then formulated as the following:

$$\underline{u} = -k_{P_{slew}}\underline{\omega_e} - k_{I_{slew}}(A_e^T - A_e)^V + \underline{\omega} \times I\underline{\omega} + I\left(A_e\frac{d\underline{\omega_d}}{dt} - \left[\underline{\omega_e}\wedge\right]A_e\underline{\omega_d}\right)$$

Where:

- $\underline{\omega_e}$=$\underline{\omega} - \underline{\omega_d}$ is the angular velocity error.
- $A_e = A_{B/N}A_d^T$ is the attitude error matrix.
- k_{P_slew}, k_{I_slew} are the gains respectively of angular velocity and attitude errors.

k_{P_slew} is the proportional term and it influences how fast the system will respond. However, a higher k_{P_slew} means a more sensitive and less stable response. On the other hand, k_{I_slew} determine how fast the steady state error is removed. A larger value will determine a larger integral action. Considering that it was adopted a manual tuning, with the following method. Firstly, it is determined how much adjustment it could be made without reaching the saturation of the actuators. Then the next step was to start with a low k_{P_slew} and no k_{I_slew}. The proportional gain was adjusted by incrementally doubling its value till the process began to oscillate. Then its value was decreased by 50%. After that the exact same process was applied to the integral gain, while keeping the value found for k_{P_slew}. At this point, the values are close to the desired ideal and it follows an implementation of a fine-tuning process.
The nonlinear control model ensures the spacecraft reaches a state where angular velocity errors ω_e are below (less than 10% error) and angular errors norm is α_e is less than 10° ($\underline{\alpha_e}$ is the vector containing angular errors).
Transformation of the computed control torque into commands for the actuators is achieved through:

$$\begin{bmatrix} V_x \\ V_y \\ -\dot{h}_z \end{bmatrix} = \begin{bmatrix} \frac{R_{nominal}}{n_{coil}A_{coil}} \\ \frac{R_{nominal}}{n_{coil}A_{coil}} \\ 1 \end{bmatrix} \odot \left(\begin{bmatrix} 0 & B_z & 0 \\ -B_z & 0 & 0 \\ B_y & -B_x & 1 \end{bmatrix}^{-1} \underline{u} \right)$$

where $\odot$ is the element-wise product and the inverse was not performed at every time step but the expression was calculated in a computationally efficient way. In this model the magnetorquers are

positioned on respectively parallel to the x and y principal axes and the reaction wheel parallel to the z axis.

6.3. 3-axis stabilization

After reaching the errors respectively $\omega_e < 0.1n$ and $\alpha_e < 10°$, a linear approximation of the control law is applied. PI controller computes the control torque based on errors in angular velocity $\left(\underline{\omega_e}\right)$ and attitude $(\underline{\alpha_e})$, supplemented by additional terms to handle non-linear factors and changes in the reaction wheel's angular momentum.

$$\underline{u} = -k_{P\_nom}\underline{\omega_e} - k_{I\_nom}\underline{\alpha_e} + \underline{\omega} \times I\underline{\omega} + k_{non\_lin}A_{RW/B}\frac{d\underline{h_{RW}}}{dt}$$

The PI gains were computed with the same strategy as before, giving however slightly different results. Furthermore, the non-linear term is considered weighted with a gain k_{non_lin}. This is due to the fact that the non-linear term influences greatly the control torque and lead the actuators to an unnecessary saturation. Therefore, the non-linear term is considered as long as saturation is prevented, thanks to the gain k_{non_lin}.
Also the 3-axis stabilization uses two magnetorquers and a reaction wheel, so the command to the actuators where computed as for the slew manoeuvre.

7. Actuators

The actuator system comprises three magnetorquers and a reaction wheel strategically incorporated to enable complete control. Indeed, it is not possible only with magnetorquers to precisely control along the axis aligned with the magnetic field. The chosen configuration (figure below) has each magnetorquer parallel to one of the principal inertia axes. In addition, the reaction wheel's rotational axis is parallel to the z principal inertia axis.

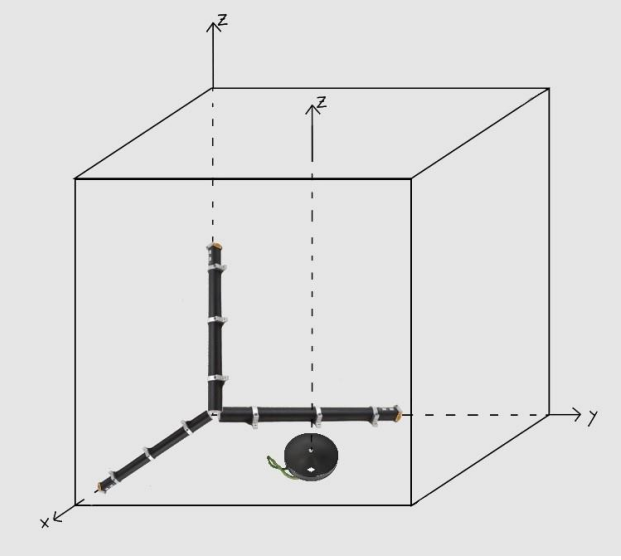

Figure 5: Actuator configuration

7.1. Magnetorquers

The chosen magnetorquer is MT120-1 from ZARM Technik with the following characteristics:

Linear dipole moment *[Am^2]*	**Linear voltage** *[V]*	**Linearity error**	**Residual dipole**	**Coil resistance** *[ohm]*	**Length** *[mm]*	**Diameter** *[mm]*	**Mass** *[kg]*
120	*14*	*<2%*	*≤0.5%*	*81.67*	*670*	*30*	*2.7*

Table 6: ZARM Technik MT120-1 specifications [4]

The unspecified data in the datasheet were either derived from provided information or obtained by referencing similar data from magnetorquers produced by the same company.
The high dipole moment ensures rapid detumbling, whereas the minimal linearity error and residual dipole facilitate precise control. Additionally, its compact dimensions and relatively low mass are well-suited concerning the satellite's overall specifications.
The model takes the voltage computed from the control as input. Utilizing a Pulse Width Modulation (PWM) controller, the model regulates the voltage delivered to the actuator by employing rapid power supply switching, ensuring the output of the PWM remains within saturation voltage values to operate effectively within the linear region. The model also accounts for changes in resistance due to design tolerances and temperature variations through a thermal model. It encompasses multiple steps, starting with the calculation of power dissipation by the resistance element based on the flow of current. This power dissipation, known as the Joule effect, leads to the generation of heat within the resistance.

$$P = \frac{V^2}{R}$$

To evaluate the resulting temperature rise, the model factors in the thermal resistance of an aluminium double-insulated wire (R_{th}). This resistance determines how efficiently the wire dissipates heat. The delta temperature, arising from this Joule heating effect, is then computed while accounting for the thermal properties of the wire material.

$$\Delta T = P \cdot R_{th}$$

Finally, the model utilizes the obtained temperature change to estimate the corresponding alteration in resistance due to temperature fluctuations. This involves considering the Temperature Coefficient of Resistance (TCR) specific to the material used in the wire. The TCR provides information on how resistance changes concerning temperature variations.

$$\Delta R = \Delta T \cdot TCR$$

By integrating these calculations, the model effectively predicts the impact of design tolerances and temperature fluctuations on resistance, offering insights into how these factors affect the system's behaviour.
Subsequently, the current is calculated using Ohm's law as $I = V/R$, and from this, the magnetic dipole ($m = In_{coil}A_{coil}$) is determined. Further linearity errors and hysteresis attributed to the residual dipole are factored in to derive the final real magnetic dipole.

7.2. Reaction wheel

The chosen reaction wheel is OCE-RW250 from OCE TECHNOLOGY with the following characteristics:

Maximum angular momentum *[Nms]*	**Maximum output torque** *[Nm]*	**Maximum speed** *[rpm]*	**Error of angular velocity** *[rad/s]*	**Dimension** *[mm]*	**Mass** *[kg]*
25	*0.2*	*3500*	*0.0164*	*312x121*	*10*

Table 7: OCE-RW250 specifications [5]

The reaction wheel is exclusively utilized during the slew maneuver and 3-axis stabilization to ensure precise control without encountering saturation. In addition, it is chosen based on dimensions and mass that align well with the overall specifications of the satellite.
The controller's output is represented by $-\dot{h}_z$. To derive the actual command for the change in angular momentum of the reaction wheel $(\underline{\dot{h}_{RW}})$, this output is multiplied by $[0; 0; -1]$. The resulting change in angular momentum is then computed, factoring in a mounting matrix and a margin for mounting error. Given that the reaction wheel can alter angular momentum solely along its rotation axis, this value is projected accordingly.
Subsequently, the model checks the torque output limit, considering the saturation derived from the maximum output torque. By dividing the projection by the wheel's inertia, the model computes the angular acceleration of the reaction wheel. Integration of this acceleration yields the angular velocity. To avoid zero condition issues associated with higher friction and potential errors, the initial angular velocity is set at $\frac{1}{4}\omega_{max}$, ensuring also ample distance from saturation. Accounting for friction, an error term opposite in sign to the angular velocity is considered. This enables the determination of the actual control torque produced by the reaction wheel.

$$T_{RW} = M_{mounting}^{-1}[(I_{RW}\dot{\omega})[0; 0; 1]]$$

Where $M_{mounting}$ is the matrix considering the mounting and the mounting error. The inverse is again not really computed but the calculation is done using the matrix multiply block on Simulink.
Further saturation checks are applied to both angular momentum and angular velocity. If the angular momentum exceeds the maximum capacity, the torque is automatically set to 0. Subsequently, a gain of -1 is employed to obtain the true control torque in body axes $-\dot{h}_z$.

7.3. Computation of the control torque

The computation of the actual control torque provided to the system dynamics varies depending on the satellite's phase. To accommodate this, the model calculates two distinct torques, feeding the appropriate one into the system dynamics based on the flags computed in the control:

- During detumbling (when $flag_{\det\_slew} = 1$): $\underline{T_{control}} = \underline{m} \times \underline{B}$
- During slew manoeuvre and 3-axis stabilization (when $flag_{\det\_slew} = 0$):

$$\underline{T_{control}} = \begin{bmatrix} 0 & B_z & 0 \\ -B_z & 0 & 0 \\ B_y & -B_x & 1 \end{bmatrix} \begin{bmatrix} m_x \\ m_y \\ -\dot{h}_z \end{bmatrix}$$

8. Results and conclusion

This section aims to present the outcomes achieved through the implementation of control strategies, divided into three distinct phases: detumbling, slew manoeuvre, and 3-axis stabilization. To assess performance, the analysis involves the utilization of the following graphs, with the vertical separating the three phases:

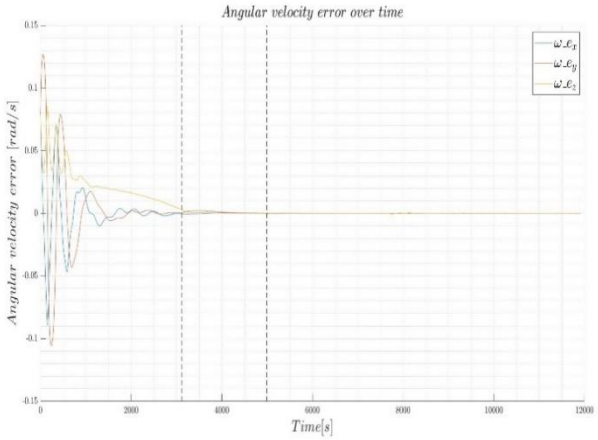

Figure 6: angular velocity error over time

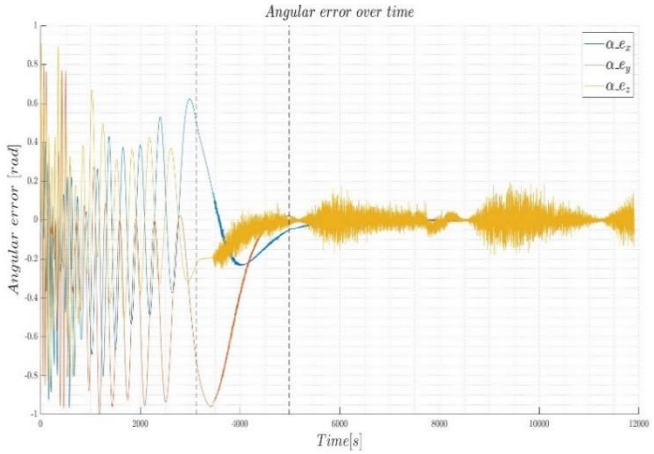

Figure 7: angular error over time

As anticipated, the angular error decreases across the three phases.
During the detumbling phase, the only focus is reducing angular velocity. As a result, angular orientation is not actively controlled. Once the slew manoeuvre is initiated, all angular errors begin to converge.

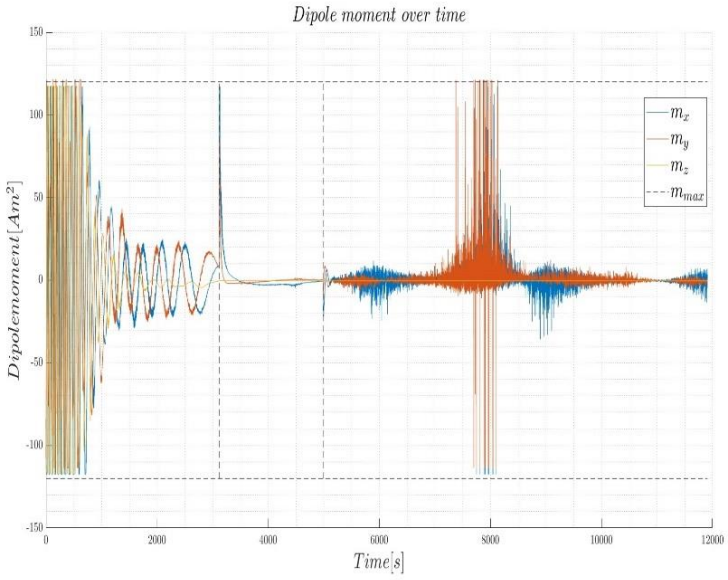

Figure 8: Magnetorquers dipole moment over time

Magnetorquers reach saturation solely at the onset of detumbling, the start of the slew manoeuvre and during a brief period within 3-axis stabilization. As these occurrences are brief and have minimal impact on the spacecraft's overall control, the suitability of the magnetorquers is approved.

The reaction wheel remains inactive until the commencement of the slew manoeuvre, thereafter, consistently operating well below its maximum torque capacity. The selection of this reaction wheel is justified by its ample saturation margin, considering that neither the angular momentum nor the angular velocity maximum thresholds are approached.

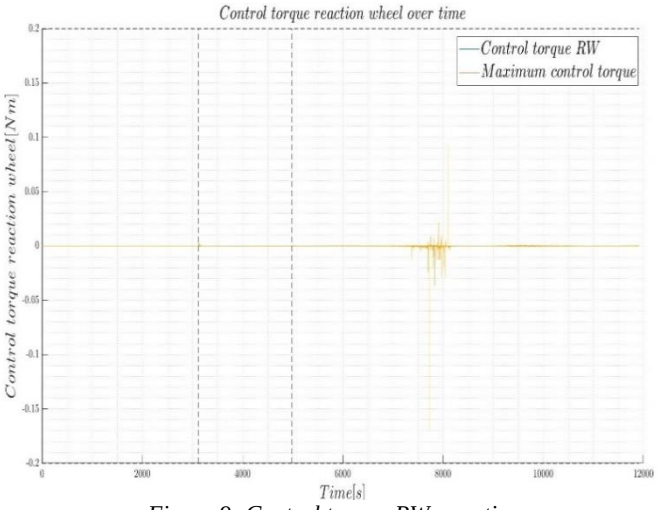

Figure 9: Control torque RW over time

8.1. De-Tumbling analysis

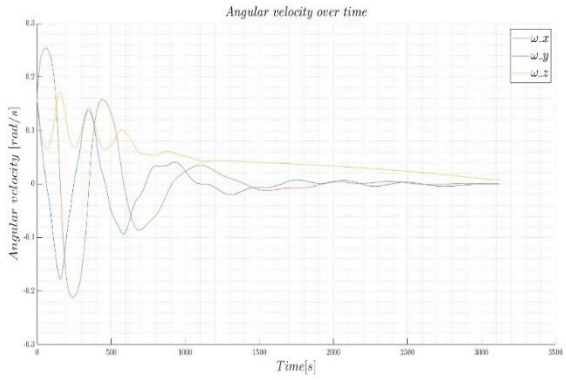

a) Angular velocity error

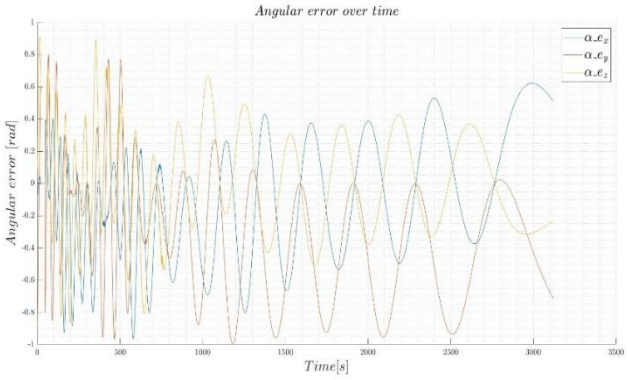

b) Angular error

The detumbling process effectively reduces the angular velocity to reach the required target.

As anticipated, angular errors remain uncontrolled during this phase. Nevertheless, it's noticeable that the oscillation period decreases across all three components as the angular velocities decrease.

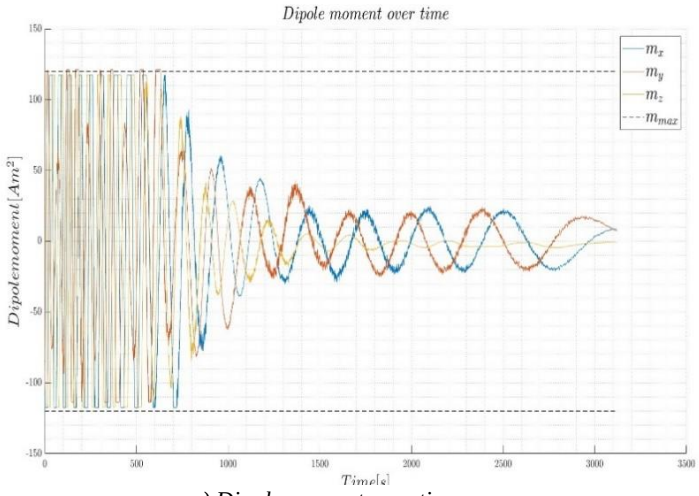

c) Dipole moment over time

Although saturation is reached in the initial phase, the detumbling process effectively reduces angular velocity. Following this brief period of saturation, the dipole moments return to the unsaturated region, allowing for a smooth completion of the detumbling process.

8.2. Slew manoeuvre analysis

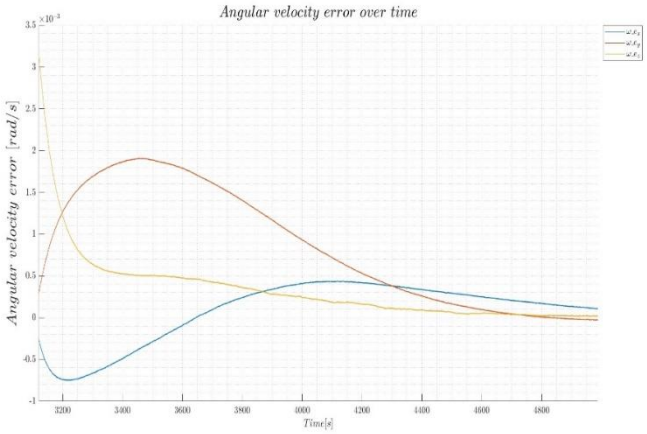

a) Angular velocity error

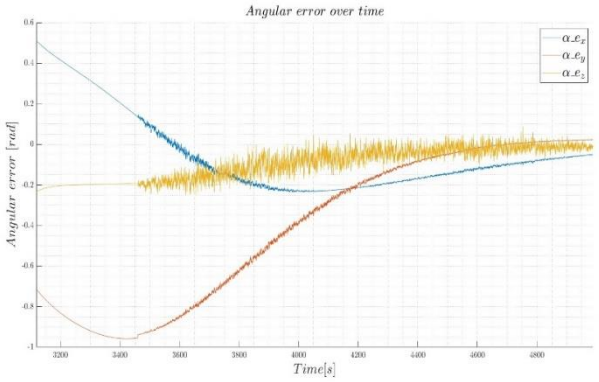

b) Angular error

The angular errors show a consistent decrease, but it's notable that during the initial control phase, the Sun sensor loses visibility of the Sun. Consequently, the kinematic attitude determination is engaged, resulting in a minor error increase over time. This discrepancy is evident in the graph's discontinuity and emphasizes the preference for Wabha's problem attitude determination under nominal conditions when the Sun is within the sensor's field of view.

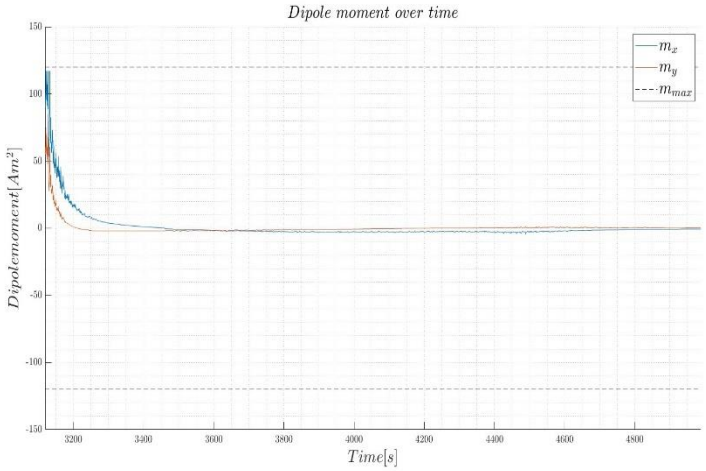

c) Dipole moment over time

After the initial phase, the magnetic dipole generated by the two magnetorquers remains considerably below its maximum capacity. This is attributed to their primary task of controlling rotations along the x and y axes, which typically involve smaller angular velocities. The selection of these magnetorquers is specifically intended to accelerate the detumbling process and facilitate the desaturation of the reaction wheel, tasks for which a higher magnetic dipole would be required.

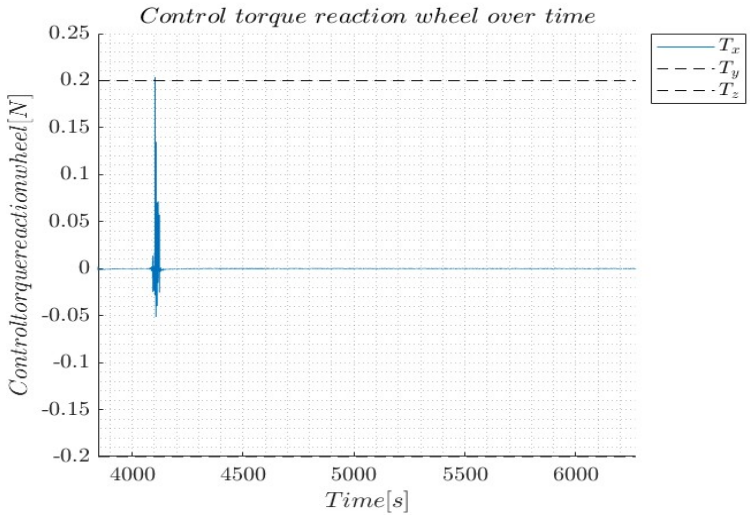

d) Control torque of the RW over time

The control torque reaches the maximum output value only once, guaranteeing control over the all phase. The high toque at around 4200s is the cause of high change at the same time in the angular velocity error graph.

8.3. 3-axis stabilization analysis

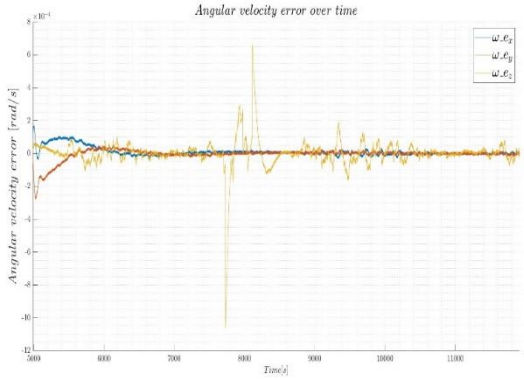

a) Angular velocity error

The angular velocity error remains minimal throughout the 3-axis stabilization phase. Around 7800s, it escalates due to a spike in control torques which briefly saturate the magnetorquers. However, the error swiftly reverts to convergence and remain limited shortly after.

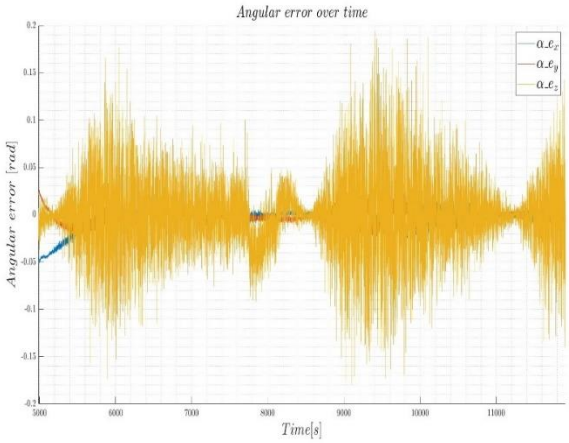

b) Angular error

The primary source of angular error arises from the z component, given that the remaining axes maintain very small angular velocities. Despite this, the maximum angular error remains below 11.45°, with a notably low mean error. This level of accuracy enables precise Nadir pointing.

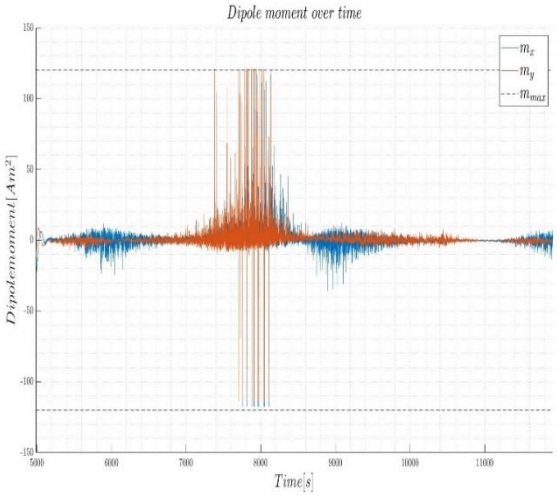

c) Dipole moment over time

As previously mentioned, at around 7800s, the magnetorquers saturate, leading to a brief period of control challenge. Following this, the control is sustained with a considerable saturation margin.

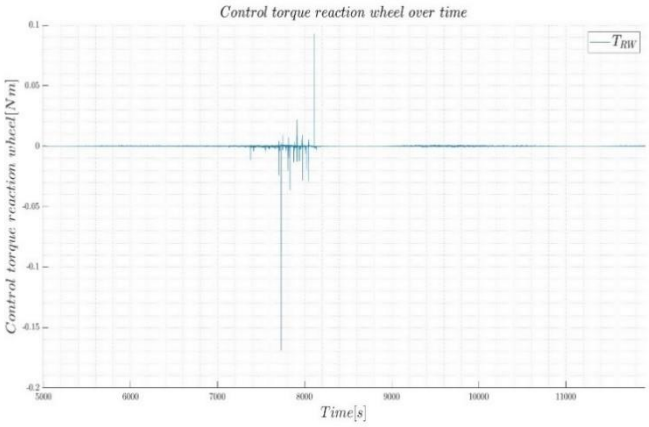

d) Control torque of the RW over time

The reaction wheel torque never reaches its maximum value (0.2 Nm) and remains consistently restricted for the majority of the phase, ensuring low power consumption. Furthermore, even at the previously mentioned crucial point for the magnetorquers, it still does not reach saturation.

9. Bibliography

[1] https://satsearch.co/products/gnssmart-gs-fog70a-gyroscope

[2] https://www.aac-clyde.space/wp-content/uploads/2021/11/MAG%C2%AD3.pdf

[3] https://www.newspacesystems.com/wp-content/uploads/2021/10/NewSpace-Sun-Sensor_20211018_2020-10e.pdf

[4] https://www.satcatalog.com/component/mt120-1/

[5] https://satsearch.co/products/oce-technology-rw250-reaction-wheel-25nms

[6] https://ntrs.nasa.gov/api/citations/19690020961/downloads/19690020961.pdf